Theory of a multimode semiconductor laser with optical feedback

T. W. Carr,[1,2] D. Pieroux,[1] and Paul Mandel[1]
[1]*Optique Nonlinéaire Théorique, Université Libre de Bruxelles, Campus Plaine, Code Postal 231, B-1050 Bruxelles, Belgium*
[2]*Department of Mathematics, Southern Methodist University, Dallas, Texas 75275-0156*
(Received 7 September 2000; published 14 February 2001)

We discuss the derivation of multimode rate equations for the description of a semiconductor laser with external cavity. We adopt a formulation where the complex field amplitudes are coupled to the nonlinear gains. For N lasing modes, this leads to $2N$ equations that display in-phased and antiphased time-dependent solutions. A simplified reference model is obtained by assuming that the key parameters are frequency independent. A general linear stability analysis leads to the prediction of two types of Hopf bifurcations. A nondegenerate Hopf bifurcation occurs with the relaxation oscillation frequency as the characteristic bifurcation frequency. A $(N-1)$-degenerate Hopf bifurcation occurs with a lower characteristic frequency. To assess the nature and stability of the solutions emerging from the Hopf bifurcations, we perform a nonlinear stability analysis on a reduced model obtained in the limit of large linewidth enhancement factor. In this asymptotic limit, the steady state is always destabilized in favor of a stable periodic inphased or antiphased state. A numerical analysis yields a bifurcation diagram of the multimode equations, which confirms the analytic results and reveals further complex regimes (quasiperiodic and chaotic, in-phased and antiphased) as the amplitude of the field fed back into the laser is increased.

DOI: 10.1103/PhysRevA.63.033817 PACS number(s): 42.55.Ah, 05.45.−a

I. INTRODUCTION

Semiconductor lasers have characteristic times much shorter than other solid-state lasers. As a result, direct characterization of the laser output is not possible and only indirect methods can be used. They produce averages in the time or in the frequency domain. In addition, the modeling of semiconductors is much more complex than the modeling of solid state lasers. There is a whole spectrum of theories varying from the purely phenomenological approach with fitting parameters to models based on the N body theory in nonequilibrium statistical mechanics [1–6]. Recently however, very fast detectors have been used to provide a time resolution of the output signal [7–11]. It appears from these experiments that in some circumstances a semiconductor laser with an external cavity (ECSL) acting as feedback operates in the longitudinal multimode regime. These results raise two questions: how do ECSL behave in the multimode regime, and why does an ECSL operate on more than one mode. In this paper, we address the first of these two questions. This question was already studied with the same purpose in mind in a recent paper [10]. Our approach differs mostly in the type of equations that are derived. A comparison between the two approaches is made at the end of Sec. II. In another set of papers [12] the dynamics of the ECSL has been analyzed without the slowly varying amplitude approximation and with proper boundary conditions. One of the results obtained in these papers is that for realistic values of the parameters, the single mode solution is stable against multimode oscillations only in a restricted domain. However, the multimode regime has not yet been studied along these lines.

The first problem is to derive a multimode extension of the Lang-Kobayashi (LK) rate equations that describe a single mode ECSL [13]. Since there is no derivation from first principles of the single mode LK equations, a generalization to the multimode regime is not obvious. This question is analyzed in Sec. II where we adopt the following strategy. We formulate the multimode rate equations for a solid-state laser in terms of complex modal field amplitudes coupled to the nonlinear gains. This is at variance with the usual formulation of the rate equations that are expressed in terms of modal field amplitudes coupled to the average population inversion and its spatial gratings. We note that in the nonlinear gain formulation, each modal field amplitude is coupled to only one nonlinear gain (associated with the same lasing cavity mode) and that the multimode feature of the laser is reflected only in a direct coupling of each nonlinear gain to all modal intensities. We transpose this structure into the LK equations to obtain their multimode extension. In the same section, we derive the steady-state solutions and focus on their linear stability. We introduce a simplified model based on the assumption that all modes have the same parameters. For this model involving N lasing modes, we show that the steady state may become unstable via two Hopf bifurcations, a nondegenerate bifurcation, and a bifurcation of degeneracy $N-1$. This result is essential because it has been shown that this property is one of the signatures of antiphase dynamics [14] and the experimental results reported in Ref. [9] give strong evidence of antiphase dynamics.

The linear stability analysis of Sec. II is limited because the multimode LK equations are far too complex. This suggests to introduce an asymptotic limit $\alpha \gg 1$ that has been successful in the analysis of single-mode ECSL [15]. In Secs. III and IV we find that to leading order the laser field can be decomposed as a sum of N independent periodic states, an inphase state and $N-1$ antiphase states. Solvability conditions determine the slow evolution of the amplitudes of these states. From the evolution equations we recover the linear stability results for $\alpha \gg 1$. We also find bifurcation equations for the periodic states, their stability and multistability, and the coexistence of the inphase and antiphase state.

In order to validate the asymptotic limit studied in Sec.

III, we have made extensive numerical simulations. Using a continuation method [16], we have determined the stability boundary of the steady state by locating all the primary Hopf bifurcation branches. Then, by integrating in time the model equations, we have found that increasing the feedback rate leads to a sequence of steady, periodic, two-frequency quasiperiodic, and finally chaotic regimes. These regimes display a clear inphase or antiphase signature, except when the chaos is of large amplitude. In Sec. V we present a summary of these simulations.

II. MULTIMODE RATE EQUATIONS

A. The Fabry-Perot cavity

The rate equations for a multimode solid-state laser [17] couple the modal complex electric field $\bar{E}_m(\bar{t})$ to the population inversion $\bar{F}(z,\bar{t})$ via the nonlinear equations

$$\frac{d\bar{E}_m(\bar{t})}{d\bar{t}}=\bar{E}_m\left\{-\gamma_{cm}+\frac{\gamma_m}{L}\int_0^L|\phi(m)|^2\bar{F}(z,\bar{t})dz\right\}, \quad (1)$$

$$\frac{\partial\bar{F}(z,\bar{t})}{\partial\bar{t}}=w(z)-\bar{F}(z,\bar{t})\left(1+\sum_p|\phi(p)|^2|\bar{E}_m(\bar{t})|^2\right), \quad (2)$$

where $\phi(m)=\sqrt{2}\sin(q_m z)$ is a lasing cavity mode. This choice of the eigenfunctions means that we formulate the rate equations for a Fabry-Perot cavity. The excitation of the population difference is modeled by the function $w(z)$. The cavity photon decay rate is γ_{cm}. The complex parameter γ_m is proportional to the linear susceptibility of the gain medium. Its real part is a measure of the linear gain and its imaginary part is related to the dispersive properties of the medium.

We first consider the single-mode regime. In solid-state laser theory, it is customary to derive from Eqs. (1) and (2) coupled equations relating the modal field amplitude $\bar{E}_m$, the average of the population inversion $\bar{D}(\bar{t})=(1/L)\int_0^L\bar{F}(z,\bar{t})dz$, and the population inversion grating $\bar{D}_m(\bar{t})=(1/L)\int_0^L\cos(2q_m z)\bar{F}(z,\bar{t})dz$, neglecting moments of the population inversion such as $\bar{D}_{m-m'}$ with $m-m'\neq 0,m$. The resulting three equations are the Tang, Statz, and deMars rate equations [18]. In semiconductor laser theory, a different formulation is preferred, which relates the complex electric field $\bar{E}_m$ to the nonlinear gain $\bar{F}_m=(2/L)\int_0^L\sin^2(q_m z)\bar{F}(z,\bar{t})dz=\bar{D}(\bar{t})-\bar{D}_m(\bar{t})$. In reduced variables, this pair of equations can be written as

$$\frac{dE_m}{dt}=(1+i\alpha)F_m E_m, \quad (3)$$

$$T\frac{dF_m}{dt}=P-F_m-(1+2F_m)|E_m|^2, \quad (4)$$

where E_m is the slowly varying field amplitude, α is the linewidth enhancement factor (or Henry factor), P is the deviation from the threshold injection current, F_m is the excess free-carrier density, and T is the ratio of the carrier density lifetime to the cavity photon lifetime. The derivation of the semiconductor laser rate equations from the general rate equations (1) and (2) is not simple. A discussion of this topic can be found in Refs. [3–5].

If an external mirror feeds a fraction η of the light back into the laser, a source has to be added to the field equation. It was shown by Lang and Kobayashi [13] that a semiconductor laser with this optical feedback can be modeled by the field equation

$$\frac{dE_m}{dt}=(1+i\alpha)F_m E_m+\eta_m E_m(t-\tau)e^{-i\Omega_m\tau}, \quad (5)$$

coupled to Eq. (4). $E_m(t-\tau)$ is the field delayed by one external cavity round trip time τ, the field phase mismatch after one round trip is $-i\Omega_m\tau$, and Ω_m is the isolated laser frequency.

In view of these results, it is clear that to generalize the LK equations to the multimode regime, the structure of Eq. (2) suggests that we simply replace Eq. (4) by

$$T\frac{dF_m}{dt}=P-F_m-(1+2F_m)\sum_n\beta_{mn}|E_n|^2, \quad (6)$$

with $\beta_{nn}=1$, while keeping Eq. (5) as it stands. The indices m and n run from 1 to N, the number of lasing modes. The cross-saturation parameters β_{mn} are related to the carrier density gratings. They are restricted to the range $0\leqslant\beta_{mn}\leqslant 1$.

A numerical analysis of Eqs. (5) and (6) has already been published [21,22]. This analysis indicates that Eqs. (5) and (6) are valid candidates to describe the multimode ECSL. Hence the more systematic approach followed in this paper.

The steady-state solution of Eqs. (5) and (6) is easy to derive in analogy with the single-mode solution. We seek steady-state solutions of the form $E_m(t)=E_m e^{i\Omega_{e,m}t}$ and $F_m(t)=F_m$. The external cavity frequency $\Omega_{e,m}$ is the shift of the lasing frequency due to the external cavity. It verifies the transcendental equation

$$\Omega_{e,m}=-\eta_m\sqrt{1+\alpha^2}\sin[(\Omega_m+\Omega_{e,m})\tau+\tan^{-1}\alpha].$$

The excess carrier density is given by

$$F_m=-\eta_m\cos[(\Omega_m+\Omega_{e,m})\tau].$$

The field intensities are the solutions of a set of N linear inhomogeneous equations

$$\sum_{n=1}^N\beta_{mn}|E_n|^2=\frac{P+\eta_m\cos[(\Omega_m+\Omega_{e,m})\tau]}{1-2\eta_m\cos[(\Omega_m+\Omega_{e,m})\tau]}.$$

At this point, we introduce a simplification that amounts to assuming that the lasing modes are distributed over a small frequency interval:

$$\beta_{mn}=\beta<1 \quad \text{for } m\neq n, \quad \eta_m=\eta, \quad \text{and } \Omega_{e,m}=\Omega_e. \quad (7)$$

It follows that $\Omega_m=\Omega$ and $F_m=F$. The assumption of equal β_{nm} amounts to the neglect of a weak dependence on the difference $n-m$ [19,20]. This becomes an exact property if consecutive modes have equal frequency differences. The experimental results reported in Ref. [9] suggest that to a very good approximation the modes are equally spaced. The choice of a constant η and $\Omega_{e,m}$ is based on the fact that the frequency difference between the lasing modes is very small compared with the optical frequency, and that most properties of the laser cavity and of the external cavity elements do not vary significantly across the optical spectrum of the lasing modes.

Given the above simplification we obtain the reference model that will be used in the remainder of this paper. The steady-state modal field intensity thus becomes

$$|E|^2=\frac{P+\eta\cos(\Delta)}{[1-2\eta\cos(\Delta)][1+\beta(N-1)]},$$

with $\Delta=(\Omega+\Omega_e)\tau$.

The linear stability of this solution can be investigated in the usual way. Seeking solutions of the multimode LK equations of the form $E_m(t)=[E+\varepsilon a_m(t)]\exp(i\Omega_e t)$ and $F_m(t)=F+\varepsilon f_m(t)$ with $0<\varepsilon\ll 1$ and where E, F, and $f_m(t)$ are real but $a_m(t)$ is complex, the linearized equations for the deviations from steady state yield the solution $a_m(t)=a_m\exp(\lambda t)$ and $f_m(t)=f_m\exp(\lambda t)$. The characteristic equation for λ is

$$D_R\times D_L^{N-1}=0, \tag{8}$$

with

$$\begin{aligned}T^{-1}D_S=&\lambda^3+\lambda^2[2\eta(1-e^{-\lambda\tau})\cos(\Delta)+2\gamma]\\&+\lambda[\eta^2(1-e^{-\lambda\tau})^2+4\eta\gamma(1-e^{-\lambda\tau})\cos(\Delta)+\Omega_S^2]\\&+2\eta^2\gamma(1-e^{-\lambda\tau})^2+\eta\Omega_S^2(1-e^{-\lambda\tau})\\&\times[\cos(\Delta)-\alpha\sin(\Delta)],\end{aligned}$$

for $S=R,L$. An alternative form of the characteristic functions D_S is given in Appendix A. Two relaxation oscillation frequencies appear in these equations

$$\Omega_R^2=\frac{2}{T}[P+\eta\cos(\Delta)],\quad \Omega_L^2=\Omega_R^2\frac{1-\beta}{1+\beta(N-1)}.$$

They are characterized by the same damping rate γ

$$\gamma=\frac{1}{2T}\frac{1+2P}{1-2\eta\cos(\Delta)}.$$

The main property to stress at this point is that any critical point arising as a zero of D_L is $(N-1)$ degenerate.

To progress in the analysis of the characteristic equation, we introduce an asymptotic limit. Semiconductor lasers with an external cavity (ECSL) normally operate in the regime $T\gg 1$, with a small feedback $\eta\ll 1$, and a large time delay $\tau\gg 1$. It has been shown [23,24] that this regime can be described by the following scaling

$$\varepsilon\equiv 1/T\ll 1,\quad \eta=O(\varepsilon),\quad P=O(1),\quad \tau=O(\varepsilon^{-1/2}), \tag{9}$$

so that $\gamma=O(\varepsilon)$. We choose η as the control parameter. In the limit (9), it is easy to verify that the steady-state solution can be destabilized by Hopf bifurcations defined by the equations $D_S(\lambda_S=\pm i\Omega_S,\eta_S)=0$. The position of the Hopf bifurcations is obtained from the equations $\mathrm{Re}[D_S(\lambda_S=\pm i\Omega_S,\eta_S)]=0$:

$$\eta_{R,L}=-\varepsilon\frac{1+2P}{[\cos(\Delta)+\alpha\sin(\Delta)]2\sin^2(\bar{\Omega}_{R,L}\tau/2)}+O(\varepsilon^{3/2}), \tag{10}$$

with

$$\bar{\Omega}_R^2=2P/T,\quad \bar{\Omega}_L^2=\bar{\Omega}_R^2\frac{1-\beta}{1+\beta(N-1)}. \tag{11}$$

The imaginary part of the characteristic equations gives the Hopf frequency

$$\Omega_{R,L}=\bar{\Omega}_{R,L}+\varepsilon\frac{1+2P}{2}\cot(\bar{\Omega}_{R,L}\tau/2)+O(\varepsilon^{3/2}).$$

From expression (10) for the critical value of the feedback parameter, it follows that the condition $\eta>0$ implies the constraint

$$\cos(\Delta)+\alpha\sin(\Delta)<0. \tag{12}$$

If this condition is verified, there is a nondegenerate Hopf bifurcation at η_R and a $(N-1)$-degenerate Hopf bifurcation at η_L. Note that if Eq. (12) is not verified, there is still the possibility that Hopf bifurcations exist, but outside the domain of parameters defined by the scaling (9). Extensive numerical simulations suggest that the steady state is always destabilized by a Hopf bifurcation if the feedback rate is large enough.

When the Hopf bifurcations occur according to Eq. (10), the nondegenerate bifurcation will be the first (i.e., $\eta_R<\eta_L$) provided

$$\sin^2(\bar{\Omega}_R\tau/2)>\sin^2(\bar{\Omega}_L\tau/2). \tag{13}$$

Otherwise, it is the degenerate Hopf associated with $D_L^{N-1}=0$ that is the first self-pulsing instability of the steady state. In the short delay limit $(\tau\to 0)$, the stability condition (13) reduces to $\bar{\Omega}_R>\bar{\Omega}_L$ which is always true and means that for $\tau\to 0$ the first instability is always the nondegenerate Hopf. The condition (13) can be written as

$$\sin\left[\sqrt{\frac{2P}{T}}\frac{\beta N}{\beta N+1-\beta}\right]\sin\left[\sqrt{\frac{2P}{T}}\frac{\beta N+2(1-\beta)}{\beta N+1-\beta}\right]>0.$$

The relevance of these results stems from the fact that the presence of a degenerate Hopf bifurcation has been shown to be a signature for antiphase dynamics [14]. This is related to the fact that there are $N-1$ different eigenvectors associated with the eigenvalue $i\Omega_L$. Because antiphase dynamics

emerges from a degenerate Hopf bifurcation, the usual theorems on the existence and stability of the time periodic solution emerging from the Hopf bifurcation no longer apply. In a recent publication [25] dealing with a different problem, it has been shown that the properties of the solutions in the vicinity of the degenerate Hopf bifurcation depend on the mode number. For instance, it was shown in that paper that for $N=3$ the emerging solutions are periodic and stable. However, for $N=4$, periodic and quasiperiodic solutions emerge, with the periodic solutions being unstable and the quasiperiodic solutions being stable. Away from the Hopf bifurcation, these two groups of solutions may exchange their stability. An explicit construction of the eigenvectors associated with the eigenvalues Ω_R and Ω_L does not seem possible at this level of description. To proceed further, we shall introduce another asymptotic limit in which this construction is feasible.

B. The ring cavity

The above formulation refers to a Fabry-Perot cavity. It is interesting to contrast the results derived in that case with the properties of a similar model set up for a ring cavity. Such a formulation has been used recently [10] to analyze the intensity statistics in the low-frequency fluctuation regime. These equations can be derived from Eqs. (1) and (2) with $\phi(m) = \exp(iq_m z)$. Proceeding exactly as for the Fabry-Perot cavity leads to $N+1$ coupled equations

$$\frac{dE_m}{dt} = (1+i\alpha)FE_m + \eta_m E_m(t-\tau)e^{-i\Omega_m\tau},$$

$$T\frac{dF}{dt} = P - F - (1+2F)\sum_n \beta_{mn}|E_n|^2,$$

where F is the space average of the excess carrier density. In a ring laser, there is no need to derive equations for the population gratings since the property $|\phi(m)|^2=1$ decouples the gratings from the field equations at this level of approximation. Hence the difference in the number of equations between the two models. The equation for F used in Ref. [10] has an additional nonlinearity that complicates the algebra but does not modify qualitatively the conclusions of the following analysis. Considering again the simplified model for which η_m, Ω_m, and β_{mn} are mode independent, it is easy to show that the linear stability analysis of the steady-state solutions is governed by the characteristic equation

$$(A\overline{A})^{N-1}D_R' = 0, \tag{14}$$

with

$$A = \lambda + \eta e^{-i\Delta}(1-e^{-\lambda\tau}), \quad \overline{A} = A(-\Delta).$$

The function D_R' differs slightly from D_R; they are identical for $\beta=1$. An explicit form of the function D_R' is given in Appendix A.

Thus, this model predicts instabilities associated with the roots of D_R' (which has a nondegenerate Hopf bifurcation) and, in addition, the roots with the degeneracy $N-1$ originating from $A\overline{A}=0$. We first consider the equation

$$\lambda + \eta e^{\pm i\Delta}(1-e^{-\lambda\tau}) = 0. \tag{15}$$

Let us determine if this characteristic equation may lead to a Hopf bifurcation. Assuming $\lambda = i\Omega$, we obtain from Eq. (15) the condition

$$i\Omega + i\eta[\pm\sin(\Delta) + \sin(\Omega\tau \mp \Delta)] + \eta[\cos(\Delta) - \cos(\Delta \mp \Omega\tau)] = 0.$$

The real part of this equation requires $\Omega\tau = 2n\pi$, which is inconsistent with the imaginary part of this equation. The same conclusion holds for the product $A\overline{A}$. Hence, this model does not support a degenerate Hopf bifurcation.

III. PHASE EQUATION ANALYSIS FOR $\alpha \gg 1$

A. Derivation

In the previous section we found isolated and $(N-1)$-degenerate Hopf-bifurcation points on the branch of steady-state solutions of the multimode-LK equations. To describe the emerging periodic solutions we follow the approach of Alsing *et al.* [15] who perform an asymptotic analysis of the single-mode case. By considering the limit $\alpha \gg 1$ they derived a third-order phase equation that can be analyzed for $T \gg 1$. Here we will summarize the application of this asymptotic method to the multimode problem and refer the reader to Ref. [15] for details of the asymptotic argument.

We make the following change of variables in Eqs. (5) and (6):

$$t \to \frac{t}{\omega}, \quad \tau \to \frac{\tau}{\omega}, \quad \omega = \sqrt{\frac{2P}{T}}, \quad b = \frac{1}{1+\beta(N-1)},$$

$$F_m = \frac{\omega}{\alpha}x_m, \quad E_m = \sqrt{bP}\left(1+\frac{1}{\alpha}y_m\right)\exp\left[i\left(\Phi_m - \frac{\Omega}{\omega}t\right)\right].$$

The resulting equations are

$$\frac{dx_m}{dt} = -\omega\xi x_m - \left(1+\frac{2\omega}{\alpha}x_m\right)b\sum_{n=1}^{N}\beta_{mn}y_n\left(1+\frac{y_n}{2\alpha}\right),$$

$$\frac{dy_m}{dt} = x_m\left(1+\frac{y_m}{\alpha}\right) + \omega\Lambda\left(1+\frac{y_m(t-\tau)}{\alpha}\right) \times \cos[\Phi_m(t-\tau) - \Phi_m], \tag{16}$$

$$\frac{d\Phi_m}{dt} = \Omega + x_m + \frac{\omega\Lambda}{\alpha}\frac{1+y_m(t-\tau)/\alpha}{1+y_m/\alpha}\sin[\Phi_m(t-\tau) - \Phi_m],$$

where

$$\Omega \to \omega\Omega, \quad \xi = \frac{1+2P}{2P}, \quad \Lambda = \frac{\eta\alpha}{\omega^2}. \tag{17}$$

In the limit $\alpha\to\infty$ the leading-order approximation to Eq. (16) is

$$\frac{dx_m}{dt} = -\omega\xi x_m - b\sum_{n=1}^{N}\beta_{mn}y_n,$$

$$\frac{dy_m}{dt} = x_m + \Lambda\omega\cos[\Phi_m(t-\tau)-\Phi_m(t)], \tag{18}$$

$$\frac{d\Phi_m}{dt} = \Omega + x_m.$$

These equations can be combined to produce N coupled third-order phase equations

$$\frac{d^3\Phi_m}{dt^3} + \omega\xi\frac{d^2\Phi_m}{dt^2} + b\sum_{n=1}^{N}\beta_{mn}\frac{d\Phi_n}{dt} - \Omega + b\Lambda\omega\sum_{n=1}^{N}\beta_{mn}\cos[\Phi_n(t-\tau)-\Phi_n(t)] = 0, \tag{19}$$

where $m=[1,N]$.

B. Leading order problem

The phase equations are analyzed in the limit $\omega\to 0$ as $T\to\infty$, while $P=O(1)$, and we look for a solution of the form

$$\Phi_m(t;\omega) = \Phi_{m0}(t,T) + \omega\Phi_{m1}(t,T) + O(\omega^2).$$

A new slow-time variable $T=\omega t$ is defined so that derivatives in t become $d/dt=\partial/\partial t+\omega\partial/\partial T$, and the delay term is expanded as

$$\Phi_{mj}(t-\tau) = \Phi_{mj}(t-\tau,T) - \omega\tau\Phi_{mjT}(t-\tau,T) + O(\omega^2\tau^2). \tag{20}$$

The leading order problem is

$$\frac{\partial^3\Phi_{m0}}{\partial t^3} + b\sum_{n=1}^{N}\beta_{mn}\frac{\partial\Phi_{n0}}{\partial t} = \Omega,$$

which has the solution

$$\Phi_{0m}(t,T) = \sum_{n=1}^{N}[A_n(T)\Psi_{mn}e^{i\omega_n t} + \text{c.c.}] + \Omega t + C_m(T),$$

$$m=[1,N], \tag{21}$$

where

$$\omega_n^2 = \omega_L^2 = (1-\beta)b, \quad \text{if } n\in[1,N-1], \tag{22}$$

$$= \omega_R^2 = 1 \quad \text{if } n=N \tag{23}$$

and

$$\Psi_{mn} = \exp[i2\pi(n/N)(m-1)]. \tag{24}$$

In Eq. (23) we have recovered the linear stability prediction for the frequencies given by Eq. (11). The solution vector Φ is composed of a sum of vectors Ψ_n weighted by A_n. For $n=[1,N-1]$ the vectors Ψ_n correspond to antiphase (AP) states, where each vector is phase shifted from the previous by $2\pi n/N$. Different Ψ_n correspond to a unique order of the phases Φ_m. When $n=N$, each element of Ψ_N equals 1 corresponding to the inphase (IP) state. The state vectors obey the relations

$$\sum_{m=1}^{N}\Psi_{mn} = U^T\Psi_n = 0 \quad \text{if } n=[1,N-1] \quad \text{(AP modes)}$$

$$= N \quad \text{if } n=N \quad \text{(IP modes)}, \tag{25}$$

where U is a column vector with each element equal to 1 [(U)nity]. These conditions appeared as ''sum rules'' in [26,27]. Orthogonality of the vectors Ψ_n follows directly from Eqs. (24) and (25). Thus, the solution vector Φ_0 has an orthogonal decomposition into AP and IP states Ψ_n weighted by A_n.

The phase $\Phi_m(t)$ depends on the slowly evolving amplitudes $A_n(T)$ and $C_m(T)$, whose time dependence can be determined from solvability conditions for the $O(\omega)$ problem. However, calculating the solvability conditions for the $A_n(T)$ is very difficult. This is because of the necessity of accounting for all possible resonant terms of the $N-1$ AP states A_n. We instead define *composite antiphase (CAP) states* as

$$B_m(T) = \sum_{n=1}^{N-1}A_n(T)\Psi_{mn} \tag{26}$$

so that $\Phi_m(t)$ may be written as

$$\Phi_{0m}(t,T) = B_m(T)e^{i\omega_L t} + A_N(T)e^{it} + \text{c.c.} + \Omega t + C_m(T),$$

$$m=[1,N]. \tag{27}$$

Orthogonality and the sum-rule property (25) of the Ψ_{mn} determine that the B_m have the properties

$$\frac{1}{N}\sum_{m=1}^{N}\Psi_{mn}B_m = A_n, \quad \sum_{m=1}^{N}B_m = 0. \tag{28}$$

Each phase $\Phi_m(t)$ has only two slowly varying amplitudes $B_m(T)$ and $A_N(T)$ for the harmonic oscillations at frequencies ω_L and 1, respectively. There are N CAP states B_m (versus $N-1$ AP states A_n) so that one is linearly dependent on the others as implied by the sum rule on the B_m; this over specification will be removed later. The slow evolution of the $B_m(T)$ will be determined by solvability conditions at $O(\omega)$.

Before proceeding to the $O(\omega)$ problem we wish to relate the evolution of the phase $\Phi_m(t)$ back to the original laser variables, the population inversion F_m, and electric field E_m. The inversion is $F_m=(\omega/\alpha)x_m=(\omega/\alpha)(d\Phi_m/dt-\Omega)$. The modal intensities $I_m=|E_m|^2$ are given in terms of y_m by

$$I_m = bP\left(1+\frac{1}{\alpha}y_m\right)^2. \tag{29}$$

In Appendix B we show that the vector $y=(y_1,\ldots,y_N)$ can be written as

$$y = -\left(\frac{d^2}{dt^2}+\omega\xi\frac{d}{dt}\right) \times\left[\sum_{n=1}^{N}\frac{R_n(\omega t)}{\omega_n^2}[\Psi_n\exp\{i[\omega_n t+\phi_n(\omega t)]\}+\text{c.c.}] + S^{-1}B(\omega t)\right], \tag{30}$$

where we have made the substitution $T=\omega t$ and the polar decomposition $A_n(T)=R_n(T)\exp[i\phi_n(T)]$. This expresses the mode intensities explicitly in terms of the slowly varying amplitudes R_n, ϕ_n, and C_m. However, our result simplifies if the amplitudes are constant because $R_{nt}=C_{mtt}=\phi_{ntt}=0$. We obtain (see Appendix B)

$$y=\sum_{n=1}^{N}\frac{R_n}{\omega_n^2}[\Psi_n\exp\{i[\omega_n t+\phi_n(\omega t)]\}+\text{c.c.}]+O(\omega). \tag{31}$$

Substituting this result in Eq. (29) we have for the intensity

$$I=bP\left(U+\frac{2}{\alpha}\sum_{n=1}^{N}\frac{R_n}{\omega_n^2}[\Psi_n\exp\{i[\omega_n t+\phi_n(\omega t)]\}+\text{c.c.}]\right) +O\left(\frac{1}{\alpha^2},\frac{\omega}{\alpha}\right). \tag{32}$$

For constant amplitude solutions, the vector of modal intensities is the steady state plus a perturbation that can be expressed as a decomposition into the AP and IP states. The total intensity is a sum of the modal intensities. Recall that $U^T\Psi_n=0$ for the AP modes so that

$$I_{\text{tot}}=\sum_{m=1}^{N}I_m=U^TI=bNP\left\{1+\frac{4}{\alpha}R_N\cos[t+\phi_N(\omega t)]\right\}. \tag{33}$$

Thus, for constant amplitudes the antiphase dynamics do not affect the magnitude of the total intensity [25].

C. The $O(\omega)$ problem

The solution to the leading-order problem depends on the slowly varying amplitudes $B_m(T)$, $A_N(T)$, and $C_m(T)$. Their evolution equations are obtained from a solvability condition on the $O(\omega)$ problem.

$$\frac{\partial^3\Phi_{m1}}{\partial t^3}+b\sum_{n=1}^{N}\beta_{mn}\frac{\partial\Phi_{n1}}{\partial t} =-3\Phi_{m0ttT}-\xi\Phi_{m0tt}-b\sum_{n=1}^{N}\beta_{mn}\Phi_{n0T} -b\Lambda\sum_{n=1}^{N}\beta_{mn}\cos[\Phi_{n0}(t-\tau)-\Phi_{n0}(t)]. \tag{34}$$

The homogeneous equation has a nontrivial solution proportional to a constant, $\exp(i\omega_L t)$ and $\exp(it)$. Terms on the right-hand side of Eq. (34) proportional to the homogeneous solutions will cause secular terms in Φ_{m1}. Solvability conditions are found by identifying the coefficients to secular terms and setting them to zero.

It is straightforward to analyze the contribution of the linear terms. The nonlinear cosine term is more difficult and we have moved the computation details to Appendix C 1. For specific values of β it is possible that resonance occurs between the antiphase states with frequency ω_L and the inphase state with relaxation frequency $\omega_R=1$. In Appendix C 2 we discuss when these resonances may occur but a study of the resulting evolution equations will not be pursued.

D. Amplitude equations

The amplitude equations for $C_m(T)$, $A_N(T)$, and $B_m(T)$ are given below where we have introduced the polar coordinates $A_N(T)=R_N(T)\exp[i\phi_N(T)]$ and $B_m(T)=S_m(T)\exp[i\varphi_m(T)]$, $m\in[1,N]$:

$$C_m(T)=-\Lambda\cos(\Omega\tau)J_0(D_I)J_0(D_m),$$

$$2A_{NT}+\xi A_N+ie^{-i\tau/2}b\Lambda\sin(\omega\tau)J_1(D_I)e^{i\phi_N(T)} \times\sum_{n=1}^{N}\beta_{mn}J_0(D_n)=0,$$

$$2B_{mT}+\xi B_m+ie^{-i\omega_L\tau/2}\frac{b}{\omega_L^2}\Lambda\sin(\omega\tau)J_0(D_I) \times\sum_{n=1}^{N}\beta_{mn}J_1(D_n)e^{i\varphi_n(T)}=0,$$

where

$$D_I=4\sin\left(\omega_R\frac{\tau}{2}\right)R_N,\quad D_m=4\sin\left(\omega_L\frac{\tau}{2}\right)S_m. \tag{35}$$

There are N composite antiphase states B_m, any one of which can be expressed as a sum of the others using Eq. (28). By summing all N solvability conditions for the B_m and using the sum property we find that

$$\sum_{n=1}^{N}J_1(D_n)e^{i\varphi_n(T)}=0. \tag{36}$$

This property can be used to eliminate B_N (i.e., D_N and φ_N) from the other $N-1$ solvability conditions. Using the polar coordinates and taking real and imaginary parts leads to

$$2R_{NT}+\xi R_N+b\Lambda\,\sin(\omega\tau)\sin\left(\frac{\tau}{2}\right)J_1(D_I)\sum_{n=1}^{N}\beta_{mn}J_0(D_n)=0, \tag{37}$$

$$2R_N\phi_{NT}+b\Lambda\,\sin(\omega\tau)\cos\left(\frac{\tau}{2}\right)J_1(D_I)\sum_{n=1}^{N}\beta_{mn}J_0(D_n)=0, \tag{38}$$

$$2S_{mT}+\xi S_m+\Lambda\,\sin(\omega\tau)\sin\left(\omega_L\frac{\tau}{2}\right)J_0(D_I)J_1(D_m)=0,$$

$$m\in[1,N-1], \tag{39}$$

$$2S_m\varphi_{mT}+\Lambda\,\sin(\omega\tau)\cos\left(\omega_L\frac{\tau}{2}\right)J_0(D_I)J_1(D_m)=0,$$

$$m\in[1,N-1]. \tag{40}$$

There are two important properties of the evolution equations that greatly simplify further analysis. First, neither R_N or the S_m depend on the phases. Second, the equations for the S_m are decoupled from each other. That is, the evolution of a particular CAP state S_m depends on itself and the inphase state A_N, but not the other S_n. The evolution equations for all the S_m are equivalent as would be expected from symmetry. As a result of these two properties, the study of the amplitude equations reduces to just two equations for R_N and any particular S_m, the $N-2$ other S_m being equivalent.

IV. ANALYSIS OF THE AMPLITUDE EQUATIONS

A. Zero solution

The zero solution $R_N=0$, $B_m=0$, $m=[1,N]$ corresponds to the steady-state solution of Eqs. (5) and (6) and identically satisfies the amplitude equations. To test its linear stability we consider R_N and B_m small and determine the eigenvalues of the linear system to be

$$\lambda_N=-\frac{1}{2}\left[\xi+2\Lambda\,\sin(\Omega\tau)\sin^2\left(\frac{1}{2}\tau\right)\right], \tag{41}$$

$$\lambda_n=-\frac{1}{2}\left[\xi+2\Lambda\,\sin(\Omega\tau)\sin^2\left(\frac{\omega_L}{2}\tau\right)\right],\quad n=[1,N-1], \tag{42}$$

where the $(N-1)$ degeneracy of the eigenvalue λ_n results from the $N-1$ equivalent CAP amplitude equations. We will see that all of the linear stability properties of the steady state are preserved by the stability of the zero solution.

If $\sin(\Omega\tau)>0$ then the zero solution is stable. However, if $\sin(\Omega\tau)<0$ bifurcations occur if $\lambda_n=0$ or $\lambda_N=0$. The former determines an $(N-1)$-degenerate bifurcation of the AP states if $\Lambda=\Lambda_A$, while the latter determines a bifurcation to the IP mode if $\Lambda=\Lambda_I$, where

$$\Lambda_{I,A}=\frac{1}{2}\,\frac{\xi}{|\sin(\Omega\tau)|\sin^2[\omega_{R,L}/2)\tau]}. \tag{43}$$

Recall that ξ is related to the pump, P, and Λ is related to the feedback strength η [see Eq. (17)]. For a fixed value of the pump, Eq. (43) indicates the value of the feedback where the steady state becomes unstable to either AP or IP periodic solutions. The IP bifurcation occurs before the AP bifurcation ($\Lambda_I\leqslant\Lambda_A$) provided

$$\sin^2\left(\frac{1}{2}\tau\right)\geqslant\sin^2\left(\frac{\omega_L}{2}\tau\right). \tag{44}$$

Because $0\leqslant\omega_L\leqslant1$, the IP mode is the first bifurcation for $\tau<\pi$ independent of ω_L. For τ fixed and $\pi\leqslant\tau\bmod 2\pi<2\pi$ (instead of $\tau\geqslant\pi$ and fixed), Eq. (44) is a condition on ω_L and hence β. In the next section we will analyze the bifurcation to the IP state followed by an analysis of the bifurcation to AP states.

Lastly, we comment on the relationship of the zero solution and its stability to the steady-state solution of Eqs. (5) and (6). In the stability analysis of the zero solution we have recovered the linear stability results of the original problem in the limit $\alpha\gg1$. Specifically, Eq. (43) for the bifurcation point is the large α limit of Eq. (10), while Eq. (44) that determines whether the bifurcation is inphase or antiphase, matches Eq. (13) exactly.

B. IP state

Assume that $\Lambda_I<\Lambda_A$ so that the primary bifurcation is to the IP state. Lasers operating in the IP state have many dynamical properties in common with single mode lasers. The IP state is defined as $B_m=0$, $m=[1,N-1]$, $R_N=R_I\neq0$, $R_{NT}=0$, where R_I satisfies the bifurcation equation

$$\Lambda=\frac{\xi}{|\sin(\Omega\tau)|\sin\left(\frac{1}{2}\tau\right)}\,\frac{R_I}{J_1(D_I)}=\frac{\Lambda_I}{2}\,\frac{D_I}{J_1(D_I)}. \tag{45}$$

In the limit $R_I\to0$ we recover the bifurcation point $\Lambda=\Lambda_I$. For $R_I\ll1$ the bifurcation equation can be approximated local to the bifurcation point as $D_I^2=8(\Lambda-\Lambda_I)/\Lambda_I$ and is supercritical. In the limit $\Lambda\to\infty$ the amplitude of the IP state takes multiple values defined by $J_1(D_I)=0$. Thus, the zeros of the $J_1(D)$ are solutions to the bifurcation equation for large feedback. The IP state bifurcates at limit points determined from the extrema of the bifurcation equation $d\Lambda/dD_I=0$. They are found to occur for D_I satisfying

$$2J_1(D_I)-D_IJ_0(D_I)=0. \tag{46}$$

Linear stability analysis will confirm that these are saddle-node (SN) bifurcations. The node solutions are the origin of the multiple-valued solutions defined by $J_1(D_I)=0$.

Linear stability is examined using $S_m=u_m$, $R_N=R_I+u_N$, and $u_m,u_N\ll1$. This linear system has an $(N-1)$-degenerate eigenvalue λ_m and an isolated eigenvalue λ_N given by

$$\lambda_m = -\frac{\xi}{2}\left[1-\frac{1}{2}\frac{\sin^2([\omega_L/2]\tau)}{\sin^2\left(\frac{1}{2}\tau\right)}\frac{D_I J_0(D_I)}{J_1(D_I)}\right], \quad (47)$$

$$\lambda_N = -\xi\left[1-\frac{1}{2}\frac{D_I J_0(D_I)}{J_1(D_I)}\right]. \quad (48)$$

The isolated eigenvalue λ_N corresponds to the variable u_N and describes the stability of the IP state with respect to an IP perturbation. When $\lambda_N=0$ we obtain the condition for limit points of the multiple solutions and examining the sign of $d\lambda_N/dD_I$ proves that these are SN bifurcations.

The CAP states become unstable when $\lambda_m=0$. However, the bifurcation point of CAP states occurs on the unstable branch of the IP solution. Hence, there are no stable antiphase solutions that bifurcate from the IP state. That is, the IP state will not become unstable due to AP perturbations and we expect the inphase solution to be preserved. An outline of a proof of this result is given in Appendix D.

C. AP state

Assume that $\Lambda_A<\Lambda_I$ so that the primary bifurcation is to the AP (CAP) state. The AP state is defined as $R_N=0$, $S_m=S_A\neq 0$, $S_{mT}=0$, where S_A satisfies the bifurcation equation

$$\Lambda = \frac{\xi}{|\sin(\Omega\tau)|\sin\left(\omega_L\frac{1}{2}\tau\right)}\frac{S_A}{J_1(D_A)} = \frac{\Lambda_A}{2}\frac{D_A}{J_1(D_A)}. \quad (49)$$

Analysis of the AP bifurcation equation yields similar characteristics as the IP bifurcation equation. Local to Λ_A the bifurcation equation is $D_A^2=8(\Lambda-\Lambda_A)/\Lambda_A$ and is supercritical. Multistability arises due to SN bifurcations (as confirmed by a stability analysis) when $2J_1(D_A)-D_AJ_0(D_A)=0$, and for $\Lambda\to\infty$ the amplitude of the AP states takes multiple values defined by $J_1(D_A)=0$.

Linear stability is examined using $S_m=S_A+u_m$, $R_N=u_N$, and $u_m,u_N\ll 1$. This linear system has an $(N-1)$-degenerate eigenvalue λ_m and an isolated eigenvalue λ_N given by

$$\lambda_m = -\xi\left[1-\frac{1}{2}\frac{D_A J_0(D_A)}{J_1(D_A)}\right], \quad (50)$$

$$\lambda_N = -\frac{\xi}{2}\left[1-\frac{1}{2}\frac{\sin^2(\tau/2)}{\sin^2([\omega_L/2]\tau)}\frac{D_A J_0(D_A)}{J_1(D_A)}\right]. \quad (51)$$

SN bifurcations that lead to multiple stability occur when $\lambda_m=0$. The isolated eigenvalue λ_N corresponds to the variable u_N and indicates that the IP state becomes unstable when $\lambda_N=0$. However, as for the antiphase bifurcation from the inphase state bifurcation of the previous section, the inphase bifurcation from the antiphase state occurs on the unstable branch of antiphase solutions and is unstable. The proof follows that presented in Appendix D.

The evolution of the CAP phases all have the same frequency since the amplitudes of the CAP states are equal. The only difference between the CAP states is due to the initial condition of the phase.

$$\varphi_m(T) = -\omega_\varphi T+\varphi_{m0}, \quad \omega_\varphi = \frac{\Lambda_A}{2}\sin(\omega\tau)\sin(\omega_L\tau). \quad (52)$$

Finally, we wish to show how the bifurcation to the CAP states relates to the original AP states. Using Eq. (26) and the sum rules for the AP state vectors, Eq. (25), and the CAP states, Eq. (28), a particular AP state is given by

$$A_n(T) = \frac{1}{N}S_A e^{-i\omega_\varphi T}\sum_{m=1}^{N}\Psi_{mn}e^{i\varphi_{m0}}, \quad (53)$$

where φ_{N0} is determined by Eq. (28). Thus, the AP bifurcation will be to a pure AP state ($A_p\neq 0$, $A_n=0$, $n\neq p$) if the initial conditions are such that the CAP states are in an antiphase configuration Ψ_p. In the next section numerical analysis finds that a pure AP state is in fact observed when the zero solution becomes unstable.

D. Summary of analysis and AP-IP coexistence

Here we focus on the case $\Lambda_A<\Lambda_I$ so that the first bifurcation is to the AP state. The same qualitative results are valid when $\Lambda_I<\Lambda_A$ and the IP state is the first bifurcation. In Fig. 1(a) we plot the bifurcation diagram of the AP state. When $\Lambda=\Lambda_A$, there is a supercritical bifurcation to the AP state. As Λ is increased, the initial branch of solutions asymptotes to a value R_A such that $J_1(D_A)=0$. Our numerical analysis in the next section describes the higher-order bifurcations and chaos that occur along this branch.

There exists SN bifurcations to AP states with different amplitudes leading to multistability. These are predicted both by the bifurcation equation (49) and the linear stability results (50). Linear stability also predicts the possibility of a combined AP and IP state solution (labeled as ''AP + IP''), where each state has nonzero amplitude. However, we can prove that this bifurcation occurs on the unstable branch of AP solutions and is unstable.

The bifurcation diagram in Fig. 1(a) describes the amplitude of the AP state when the amplitude of the IP state is zero. We now consider the properties of a nonzero IP state, with zero AP state, that bifurcates from the zero solution if $\Lambda=\Lambda_I$. The results are shown in Fig. 1(b). We still assume that $\Lambda_A<\Lambda_I$ so that the AP state is the first bifurcation. Hence, the zero solution is unstable when $\Lambda=\Lambda_I$ and we expect the IP state to be unstable. To be more precise we examine the eigenvalues for the stability of the IP state given by Eqs. (47) and (48). The eigenvalue λ_N, given by Eq. (48), is 0 at the bifurcation point and is negative along the branch of IP solutions. However, the eigenvalue λ_m is positive at the IP bifurcation point so that the IP state is unstable. To see this take the limit as $D_I\to 0$:

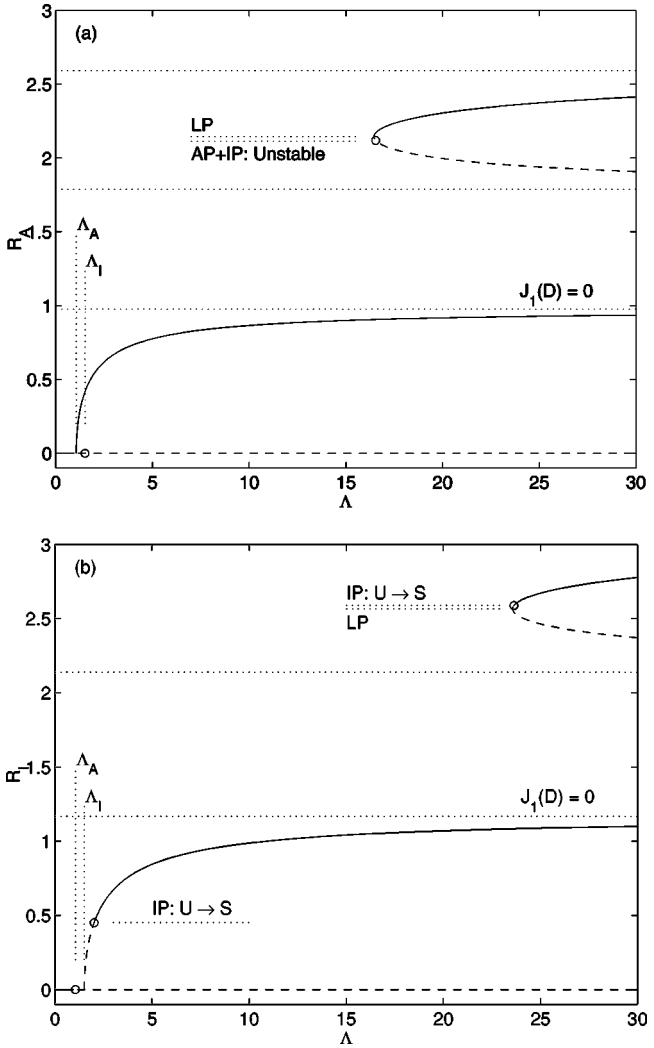

FIG. 1. Analytical bifurcation diagrams illustrating the case $\Lambda_A<\Lambda_I$. (a) $R_A\neq 0$, $R_I=0$, (b) $R_A=0$ and $R_I\neq 0$. ''AP + IP'' indicates the secondary bifurcation described by $R_A\neq 0$ and $R_I\neq 0$ that occurs on the saddle branch of solutions and is unstable. ''IP: U $\rightarrow$S'' indicates a bifurcation point where the nonzero IP state becomes stable. Fixed parameters: $\xi=2$, $\beta=0.8$, $\omega=0.022\,36$, and $\tau=\Omega=35.777$.

$$\lim_{D_I\rightarrow 0}\lambda_m=-\frac{\xi}{2}(1-r),\quad r=\frac{\sin^2(\omega_L\tau/2)}{\sin^2(\tau/2)}. \tag{54}$$

Because $\Lambda_A<\Lambda_I$, $r>1$ and $\lambda_m>0$.

The eigenvalue λ_m does not remain positive. The quantity $D_IJ_0(D_I)/J_1(D_I)$ is a decreasing function of D_I so that the IP state becomes stable when D_I increases to a value such that

$$\frac{D_IJ_0(D_I)}{J_1(D_I)}=\frac{2}{r}. \tag{55}$$

The change from an unstable to stable IP state occurs (i) on the branch of solutions emanating from $\Lambda=\Lambda_I$, and (ii) on the upper branch of solutions emanating from the limit points. This can be proved using arguments similar to those developed in Appendix D. These points are labeled as ''IP: U$\rightarrow$S'' (unstable to stable) in Fig. 1(b). Thus, for certain Λ there is a coexistence of AP states and IP states described by $R_A\neq 0$, $R_I=0$ and $R_A=0$, $R_I\neq 0$, respectively.

As Λ is increased, the zero state will bifurcate to an AP periodic state. For high values of Λ the antiphase attractor displays a crisis and becomes in phase, as described in the next section. Upon decreasing Λ the system returns along the inphase branch described above and shown in Fig. 1(b). However, the IP state loses stability when D_I satisfies Eq. (55) and will return to the AP state. In the next section we show that the sequence of bifurcations predicted by the asymptotic analysis is exhibited by the simulation of the original system.

V. NUMERICAL RESULTS

In this section, we check the validity of the analytical results of the previous sections. This is necessary because these results have been derived under the double assumption $\alpha\rightarrow\infty$ and $T\gg 1$. Next, we analyze the dynamics of the full and reduced models given by Eqs. (16) and Eqs. (18), respectively, beyond the first Hopf bifurcation.

To obtain our numerical results, we used a continuation method and intensive numerical integration. For the former, we used DDE-BIFTOOL, a MATLAB package dedicated to the continuation of delay-differential equations [16]. For the latter, we used a variable step-size Runge-Kutta 4(3) integration scheme with Hermite interpolation [29]. All the numerical experiments were carried out with $T=2000$, $P=1/2$, and $\tau=1600$, or equivalently $\xi=2$, $\omega\approx 0.022\,36$, $\tau=\Omega\approx 35.777$, as fixed parameters. For the full model, we chose $\alpha=5$. We focused on the three and four-mode cases.

In the previous sections, we show that the laser steady state is destabilized by a Hopf bifurcation leading to a periodic regime if $\Lambda=\eta\alpha/\omega^2$ is increased beyond Λ_I or Λ_A. According to Eqs. (43) and (44), the emerging periodic regime is inphase or antiphase, depending on the value of β. To check that prediction, we plot in Fig. 2 the Hopf bifurcation branches in the parameter space (Λ,β) for a three-mode system. The full curves correspond to the full model, the dotted curves to the reduced model, and the dashed curves to the asymptotic predictions given by Eq. (43). The curves characterized by Λ constant correspond to Hopf bifurcations from which an inphase periodic solution emerges. The other curves that fold back about $\Lambda=1$ correspond to $(N-1)$-degenerate Hopf bifurcations from which an antiphase periodic solution emerges. As can be seen, the dotted curves are almost indistinguishable from their corresponding full curves. This demonstrates that neglecting the terms of order $1/\alpha$ and $1/\alpha^2$ in Eqs. (16) has little effect on the location of the primary Hopf bifurcation points.

Equations (43) and (44) that result from Eqs. (18) by taking advantage of the large value of T, successfully predict the main features of the bifurcation curves, even if a quantitative discrepancy can be noticed between the dashed curves and the corresponding full and dotted curves. This discrepancy originates from the expansion of the delayed term in Eq. (20). This expansion is justified only if $\omega\tau\ll 1$. However, for

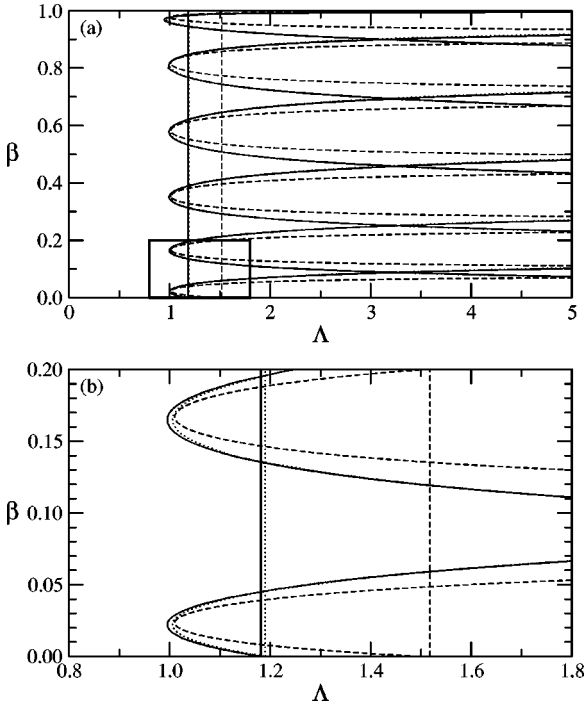

FIG. 2. (a) Hopf bifurcation curves in the (Λ, β) parameter space for $N=3$ modes. The full lines are obtained numerically from the full model Eqs. (16) with $\alpha=5$. The dotted lines are obtained numerically from the reduced model Eqs. (18). The dashed lines correspond to the analytical predictions of Eq. (43). (b) Enlargement of the box in (a). Fixed parameters: $\xi=2$, $\omega=0.022\,36$, and $\tau=\Omega=35.777$.

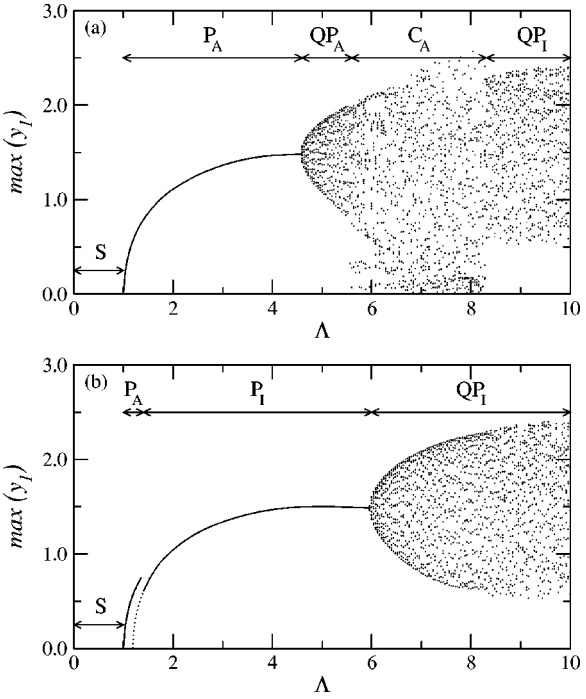

FIG. 3. Forward (a) and backward (b) bifurcation diagrams of the reduced model Eqs. (18) for $N=3$ modes. The local maxima of $y_1(t)$ are plotted versus the feedback parameter Λ. Labels *S*, *P*, *QP*, and *C* design, respectively, steady, periodic, quasiperiodic, and chaotic regimes. The subscript I (respectively, A) means inphase (respectively, antiphase). Only the stable regimes are plotted, but for the dotted part of the P_I branch that is unstable. Fixed parameters: *same as in Fig. 1.*

the values of parameters we use here, $\omega\tau\approx0.8$. We have checked that a better quantitative agreement was achieved for $\omega\tau\approx0.4$. For larger values of $\omega\tau$, Eq. (20) is not valid anymore and the delayed term $\Phi_{mj}(t-\tau,T-\omega\tau)$ must be retained. This leads to amplitude equations that are still delay-differential equations as in Ref. [30].

For each set of curves, i.e., full, dotted, or dashed, Fig. 2 shows that the inphase curve has two common points with each antiphase curve. At such a point, the inphase and antiphase Hopf bifurcations collide and the branches of periodic solutions emerging from these bifurcations exchange stability. As magnified in Fig. 2(b), a bifurcation collision occurs at $\beta=0$ for the three sets of curves. This is expected since the modes of the system are totally decoupled at $\beta=0$ and the laser dynamics displays most likely a combination of inphase and antiphase oscillations.

A typical bifurcation diagram is presented in Fig. 3. It is obtained from the reduced model Eqs. (18) for $N=3$ modes and $\beta=0.8$. The top (bottom) diagram is drawn by increasingly (decreasingly) sweeping Λ. At each change of Λ, a small amplitude noise is added to the current solution before letting the system relax towards its new regime. Without noise, the switch from a solution with equal y_i to a solution with unequal y_i would be impossible with our numerical integrator. Adding noise also helps the system to move away from a branch that just changed from stable to unstable.

Figure 3 also demonstrates bistability between the inphase and antiphase regimes. As shown in Fig. 2, a two-degenerated Hopf bifurcation located at $\Lambda\approx1$ destabilizes the steady state in favor of an antiphase periodic regime [Fig. 4(a)]. This regime is stable up to $\Lambda\approx4.6$. It is then destabilized by a torus bifurcation from which an antiphase quasiperiodic solution emerges [Fig. 4(b)]. At $\Lambda\approx5.6$, the regime becomes slightly chaotic [Fig. 4(c)]. The chaotic attractor evolves while sustaining antiphase oscillations [Fig. 4(d)]. It is destroyed at $\Lambda\approx8.3$ and is replaced by an inphase chaotic regime [Fig. 4(e)].

Increasing Λ further, the inphase chaos evolves into a full developed chaos where inphase and antiphase features are both present [Fig. 4(f)]. If Λ is decreased from there, the regime returns to the inphase chaos followed by an inphase quasiperiodic regime [Fig. 4(g)]. The inphase quasiperiodic regime maintains until it vanishes at a torus bifurcation for $\Lambda\approx6$. At that value, the regime becomes inphase periodic [Fig. 4(h)]. Decreasing further Λ down to $\Lambda\approx1.4$, the periodic regime is destabilized by a two-degenerated Hopf bifurcation, as predicted by the asymptotic analysis [see Fig. 1(b)]. At that bifurcation, the laser regime jumps onto the antiphase branch. As shown in Fig. 2, the branch of unstable inphase periodic regime [indicated by a dotted curve in Fig. 3(b)] joins the branch of steady states at $\Lambda\approx1.2$.

It is worthwhile to note that $y_1=y_2=y_3$ in the miscellaneous inphase regimes described above. Moreover, the antiphase regimes are of the AD1 type, i.e., each mode displays the same behavior shifted from one another [26,27]. The dy-

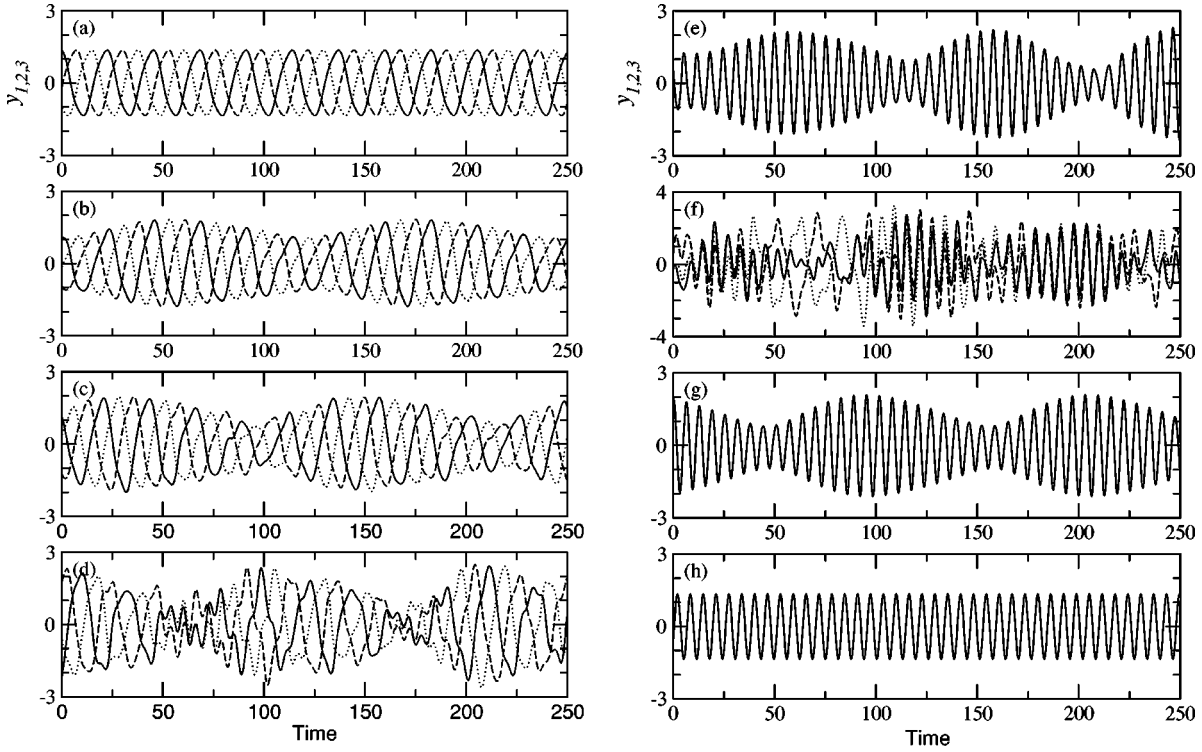

FIG. 4. Temporal time traces of y_1, y_2, and y_3 displayed by the reduced model Eqs. (18) for $N=3$ modes. Value of Λ: (a) 3, (b) 5, (c) 5.6, (d) 8, (e) 9, (f) 18, (g) 7, and (h) 3. Regimes (a)–(d) and regimes (e)–(h) are localized on the antiphase and inphase branches, respectively. See the main text for a thorough description. Other fixed parameters: *same as in Fig. 1*.

namics of the full model [Eqs. (16)] with $\alpha=5$, is very similar to that of the reduced model. However, it displays two regimes that are absent in the $\alpha\to\infty$ case. First, the antiphase quasiperiodic regime locks into a periodic regime for $6.2 \leqslant \Lambda \leqslant 6.7$ [Fig. 5(a)]. The end of the locking area corresponds to the appearance of chaos. Secondly, there are now inphase solutions with unequal y_i [Fig. 5(b)].

For $\beta=0.9$, we have checked that the laser bifurcates from the steady state to an inphase periodic state, conforming to the prediction of Fig. 2. Moreover, we have found two other inphase branches that coexist with the main one. Their domain of stability is $14.1<\Lambda<18.0$ and $15.2<\Lambda<18.6$, respectively. The system can thus display multistability between three different inphase regimes. The two extra branches present the same dynamical sequences as the main inphase branch: from steady to periodic to quasiperiodic to chaotic regime. Switching between the three branches as Λ is varied has been observed. For $\beta=0.9$ and $0<\Lambda<20$, we found no stable antiphase regime. Only the chaotic regime presents a partial antiphase feature similar to that shown in Fig. 4(g).

Finally, two other kinds of antiphase dynamics have been noticed for four-mode systems. The first one is illustrated in Fig. 5(c). The four modes group into two clusters where $y_1=y_2$ and $y_3=y_4$ (or any other configuration obtained by permutation of the y_i). This is an example of AD2 regime [26,27]. In the second case, displayed in Fig. 5(d), the four modes group also into two clusters, but the modes in one of the clusters display small differences.

VI. DISCUSSION

The recent experiments that have been reported on the observation of multimode regimes in ECSL are the motivations of this paper. They force the consideration of the multimode extension of the Lang-Kobayashi (LK) equations. This extension is not unique and therefore models must be scrutinized and confronted with experiments for validation.

The first problem that arises is the derivation of a multimode extension of the LK equations. The problem stems from the fact that the LK equations are phenomenological equations. Fortunately, they are rate equations, implying a fairly low level of sophistication in the physical description. We have derived Eqs. (5) and (6) by analogy with the multimode solid-state laser theory in the rate equation approximation.

Another difficulty is related to the experimental observation of antiphase regimes that are necessarily multimode. In solid-state lasers with homogeneous broadening, multimode regimes are not possible in the ring configuration. They require population gratings or spatial holes burned in the population inversion profile. This effect is produced by the spatial inhomogeneity of the field intensity (and not the field amplitude), as is the case in a Fabry-Perot cavity. The physics of semiconductor lasers is much more complex and the spatial grating is usually neglected on the grounds that diffusion should wash it out. Though it is clear that diffusion will reduce the role of the gratings, the very existence of multimode regimes suggests that some residual effects remain and have a profound influence on the laser dynamics. Our ap-

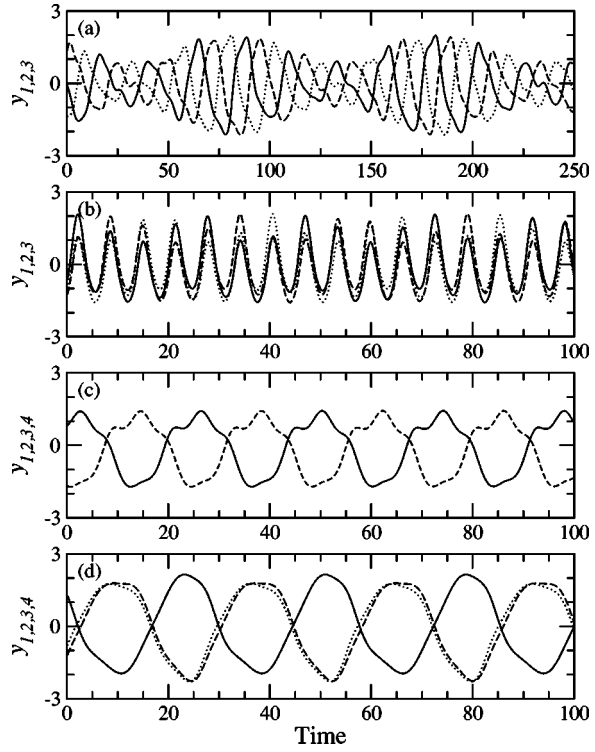

FIG. 5. Temporal time traces of the y_i. (a) $N=3$ modes, full model Eqs. (16): locking of the antiphase quasiperiodic regime. $\alpha=5$, $\beta=0.8$, and $\Lambda=6.5$. (b) $N=3$ modes, full model: inphase quasiperiodic regime with $y_1\neq y_2\neq y_3$, $\alpha=5$, $\beta=0.8$, and $\Lambda=6.0$. (c) $N=4$ modes, full model: AD2 periodic regime with $y_1=y_2$ and $y_3=y_4$, $\alpha=5$, $\beta=0.75$, and $\Lambda=4.0$. (d) $N=4$ modes, reduced model Eqs. (18): AD2-like periodic regime with $y_1=y_2$ and $y_3\approx y_4$. $\beta=0.85$ and $\Lambda=7.0$. Other fixed parameters: *same as in Fig. 2*.

proach has been fully phenomenological, using the experimental facts to motivate a multimode description of the ECSL. However, there remains to derive, in a more fundamental way, these multimode equations to understand which balance of linear and nonlinear processes dominates the physics of these devices.

In order to simplify somewhat the analysis of the multimode ECSL rate equations (5) and (6), we have introduced a reference model by assuming the mode independence of three key parameters (7).

A linear stability analysis of the steady-state solutions has been performed both for general parameters and in the asymptotic limit $\alpha\gg 1$, $T\gg 1$. The latter is from the analysis of evolution equations derived to describe the bifurcating periodic solutions. The results of the two analyses are consistent with each other. The destabilization of the steady state due to a Hopf bifurcation depends on the delay and on the cross-saturation parameter, and the cross-saturation parameter plays a critical role in determining if the first bifurcation is to inphase or antiphase periodic solutions.

The periodic solutions that bifurcate from the steady state are analyzed using the asymptotic limit $\alpha\gg 1$. To leading order we find that the laser intensity output can be decomposed into an IP state and $N-1$ AP states whose amplitudes evolve according to solvability conditions determined at higher order. The dynamics of the IP state are identical to the single-mode laser and we reproduce the results of Alsing *et al.* [15]. Namely, the bifurcation is supercritical, and for large feedback, there are saddle-node bifurcations leading to multistability.

Determining the solvability conditions for the AP states is extremely difficult and can be done only approximately. However, progress can be made by introducing the ''composite antiphase states'' for which we can derive exact solvability conditions. The bifurcation results are similar to the IP state in that the AP bifurcation is supercritical and there exists critical feedback strengths where multistability appears. The drawback of the CAP states is that we can no longer differentiate between the $N-1$ AP states. We cannot test the stability of one AP state with respect to another, and so cannot say whether one, two, or all $N-1$ AP states will bifurcation at Λ_A. However, our method has been very successful in describing the competition between the IP and AP states.

In previous studies of antiphase dynamics in solid-state lasers, it has been found that the AP dynamics is periodic or quasiperiodic, depending on the number of modes N [25]. For the semiconductor laser with delay that is considered here, the initial bifurcation is always to a periodic state. Quasiperiodic solutions occur for higher levels of feedback as secondary bifurcations.

Of particular importance is the competition between the IP and AP states. We can provide explicit conditions for which will be the first bifurcation. Numerical analysis has shown that for large feedback, higher-order bifurcations cause a system that was initially antiphase to exhibit inphase dynamics after the crisis of the antiphase attractor. Surprisingly, when the feedback is decreased, the system exhibited IP periodic solutions. Our bifurcation study has shown that even when the first bifurcation is AP, for example, there are coexisting branches of IP solutions. Hence, the jump from the IP to AP state for decreasing feedback, as seen in the numerical simulations, is well predicted by a definite bifurcation point.

Finally, the analytical predictions have been confirmed by a numerical approach on both the full equations (16) and the $\alpha\gg 1$ approximate equations (18). Using a continuation method for delay-differential equations, we have determined the location and type of bifurcation points. The numerical results were in excellent agreement with the analytical predictions. The main observed regimes have also been described. The periodic, quasiperiodic, and lightly chaotic regimes exhibit always a clear inphase or antiphase signature. We have observed no local bifurcation allowing for the reversible switch from inphase to or from antiphase.

ACKNOWLEDGMENTS

This research was supported by the Fonds National de la Recherche Scientifique and the Interuniversity Attraction Pole program of the Belgian government. T.W.C. also acknowledges support from National Science Foundation

Grant No. DMS-9803207. Fruitful discussions with E.A. Viktorov and J.R. Tredicce are gratefully acknowledged.

APPENDIX A: THE CHARACTERISTIC FUNCTIONS

The characteristic equations (8) and (14) obtained from the linear stability analysis of Sec. II depend on three functions, D_R, D_L, and D_R', which can be written as

$$D_R=(1-\beta+N\beta)(\bar{A}B+AB^*)C+A\bar{A}D,$$

$$D_L=(1-\beta)(\bar{A}B+AB^*)C+A\bar{A}D,$$

$$D_R'=N(\bar{A}B+AB^*)C+A\bar{A}[D+2E^2(1-\beta)(N-1)],$$

in terms of the functions

$$A=\lambda+\eta e^{-i\Delta}(1-e^{-\lambda\tau}),\quad \bar{A}=A(-\Delta),$$

$$B=(1+i\alpha)E, C=(1+2F)E,$$

$$D=\lambda T+1+2E^2(1-\beta+\beta N).$$

APPENDIX B: INTENSITIES

The vector $y=(y_1,\ldots,y_N)$ can be written as

$$y=-\frac{1}{b}\left(\frac{d^2}{dt^2}S^{-1}\cdot\Phi+\omega\xi\frac{d}{dt}S^{-1}\cdot\Phi-\xi\Omega S^{-1}\cdot U\right),$$

where S is the cross-saturation matrix, whose elements are given by β_{mn}; hence, S is 1 on the diagonal and β in every off diagonal element.

The cross-saturation matrix can be decomposed as

$$S=(1-\beta)I_d+\beta UU^T,$$

where I_d is the usual identity matrix. The advantage of this expression for S is that it is easy to compute $S\cdot\Psi_n$ because the action of U^T on the Ψ_n is known from Eq. (25). It also allows us to obtain the inverse of S as

$$S^{-1}=\frac{1}{1-\beta}I_d-\frac{b\beta}{1-\beta}UU^T.$$

With this result we can determine $S^{-1}\cdot\Phi$ and then y is given by

$$y=-\left(\frac{d^2}{dt^2}+\omega\xi\frac{d}{dt}\right)\times\left[\sum_{n=1}^{N}\frac{R_n(\omega t)}{\omega_n^2}[\Psi_n\exp\{i[\omega_n t+\phi_n(\omega t)]\}+\text{c.c.}]+S^{-1}\cdot B(\omega t)\right],\tag{B1}$$

where we have made the substitution $T=\omega t$. This expresses the mode intensities explicitly in terms of the slowly varying amplitudes R_n, ϕ_n, and C_m. The result simplifies if the amplitudes are constant because $R_{nt}=C_{mtt}=\phi_{ntt}=0$. From Eq. (B1) we obtain

$$y=-\sum_{n=1}^{N}\frac{R_n}{\omega_n^2}\left[\Psi_n\left[i\omega\xi\left(\omega_n+\frac{d\phi_n}{dt}\right)-\left(\omega_n+\frac{d\phi_n}{dt}\right)^2\right]\times\exp\{i[\omega_n t+\phi_n(\omega t)]\}+\text{c.c.}\right]-\omega\xi S^{-1}\cdot\frac{dB}{dt},$$

where $d\phi_n/dt$ and dB/dt are $O(\omega)$ constants. But because $\omega\ll 1$ we have

$$y=\sum_{n=1}^{N}\frac{R_n}{\omega_n^2}[\Psi_n\exp\{i[\omega_n t+\phi_n(\omega t)]\}+\text{c.c.}]+O(\omega),\tag{B2}$$

where we have used the property that the derivatives of ϕ and B are $O(\omega)$.

APPENDIX C: COMPUTING THE SOLVABILITY CONDITION

1. Nonlinear contribution

We now present some of the computational details leading to the solvability conditions. The amplitudes in polar coordinates are $A_n(T)=R_n(T)\exp[i\phi_n(T)]$ and $B_m(T)=S_n(T)\exp[i\varphi_n(T)]$. The phase difference can then be written as

$$\Phi_{n0}(t-\tau)-\Phi_{n0}(t)=-\Omega\tau+D_I\sin(\theta_I)+D_n\sin(\theta_n),$$

$$D_I=4\sin\left(\omega_R\frac{\tau}{2}\right)R_N,\quad Q_n=4\sin\left(\omega_L\frac{\tau}{2}\right)S_n,\tag{C1}$$

$$\theta_I=\left(t-\frac{\tau}{2}\right)+\phi_N,\quad \theta_n=\left(t-\frac{\tau}{2}\right)+\varphi_n,$$

so that

$$\cos[\Phi_{n0}(t-\tau)-\Phi_{n0}(t)]=\cos(\Omega\tau)\cos[D_I\sin(\theta_I)+D_n\sin(\theta_n)]+\sin(\Omega\tau)\sin[D_I\sin(\theta_I)+D_n\sin(\theta_n)].$$

Use the identity [28] [Eqs. (9.1.2) and (9.1.43]

$$\exp[iD\sin(\theta)]=\sum_{k=-\infty}^{\infty}J_k(D)e^{ik\theta},$$

where J_k is the order k Bessel function of the first kind. Then

$$\cos[\Phi_{n0}(t-\tau)-\Phi_{n0}(t)]$$
$$=\cos(\Omega\tau)\mathrm{Re}\left\{\left[\sum_{k=-\infty}^{\infty}J_k(D_I)\exp(ik\theta_I)\right]\times\left[\sum_{k=-\infty}^{\infty}J_k(D_n)\exp(ik\theta_n)\right]\right\}+\sin(\Omega\tau)\mathrm{Im}[\ \ldots\ ].$$

Expanding the products, we collect terms proportional to constants, $\exp i\omega_L t$ and $\exp it$. Extra care is necessary if resonances between the two frequencies are to be considered (see Appendix C 2).

The calculation of the nonlinear term is completed by noting that

$$\sum_{n=1}^{N}\beta_{mn}\cos[\Phi_{n0}(t-\tau)-\Phi_{n0}(t)]$$

corresponds to the cross-saturation matrix S operating on the acting on the cos of the phase difference.

2. Resonances

Additional secular terms will be produced if there is a resonance relationship between the modes $\exp(i\omega_L t)$ and $\exp(it)$. There is not a primary resonance $\omega_L=1$ for $\beta\neq 0$. However, higher-order resonances $(p/q)\omega_L=1$ $(p\neq q,\ p$ and q integers) are possible if

$$\beta=\frac{p^2-q^2}{p^2+q^2(N-1)},\quad p>q. \tag{C2}$$

We expect the strongest resonance to be when $(p,q)=(2,1)$, which occurs for $\beta=3/(3+N)$. For the present analysis we assume that β is tuned away from resonances.

APPENDIX D: STABILITY OF THE IP STATE

Outline of proof

Let

$$G=\frac{D_I J_0(D_I)}{J_1(D_I)},\quad r=\frac{\sin^2[(\omega_L/2)\tau]}{\sin^2\left(\frac{1}{2}\tau\right)}.$$

Then

$$\lambda_n=-\frac{\xi}{2}\left[1-\frac{1}{2}rG\right],\quad \lambda_N=-\xi\left[1-\frac{1}{2}G\right].$$

The AP bifurcation point and the SN bifurcation point are determined by $\lambda_n=0$ and $\lambda_N=0$, respectively. The bifurcation points occur when

$$\text{AP:}\quad G\equiv G_A=\frac{2}{r},\quad \text{SN:}\quad G\equiv G_I=2.$$

Because $\Lambda_I<\Lambda_A$, we have from Eq. (44) that $r\leqslant 1$ and so $G_A\geqslant G_I$; the value of G at the AP bifurcation is greater than or equal to the value of G at the SN bifurcation. It can be shown that G is a decreasing function of D_I on any interval where G is continuous. Thus, D_I at the SN bifurcation point is greater than or equal to the value of D_I at the AP bifurcation. Thus, the AP bifurcation occurs on the lower branch of solutions emanating from the SN bifurcation point. Linear stability indicates this is the unstable branch.

[1] *Nonlinear Dynamics of Semiconductor Lasers*, D. Lenstra, Guest Editor, Quantum Semiclassic. Opt. **5**, 655 (1997).

[2] M. Osinski, P. Blood, and A. Ishibashi, Proc. SPIE **3625** (1999).

[3] G.P. Agrawal, *Long Wavelength Semiconductor Lasers* (Van Nostrand Reinhold, New York, 1986).

[4] H. Haug and S.W. Koch, *Quantum Theory of the Optical and Electronic Properties of Semiconductors* (World Scientific, Singapore, 1990).

[5] W.W. Chow, S.W. Koch, and M. Sargent III, *Semiconductor-Laser Physics* (Springer-Verlag, Heidelberg, 1994).

[6] G.H.M. van Tartwijk and D. Lenstra, Quantum Semiclassic. Opt. **7**, 87 (1995).

[7] G. Huyet, S. Balle, M. Giudici, C. Green, G. Giacomelli, and J. Tredicce, Opt. Commun. **149**, 341 (1998).

[8] G. Huyet, S.P. Hegarty, M. Giudici, B. de Bruyn, and J.G. McInerney, Europhys. Lett. **40**, 619 (1997).

[9] G. Vaschenko, M. Giudici, J.J. Rocca, C.S. Menoni, J. Tredicce, and S. Balle, Phys. Rev. Lett. **81**, 5536 (1998).

[10] D.W. Sukow, T. Heil, I. Fischer, A. Gavrielides, A. Hohl-AbiChedid, and W. Elsäßer, Phys. Rev. A **60**, 667 (1999).

[11] I. Wallace, Dejin Yu, R.G. Harrison, and A. Gavrielides, Quantum Semiclassic. Opt. **2**, 447 (2000).

[12] A.A. Duarte and H.G. Solari, Opt. Commun. **144**, 99 (1997); Phys. Rev. A **58**, 614 (1998); **60**, 2403 (1999).

[13] R. Lang and K. Kobayashi, IEEE J. Quantum Electron. **QE-16**, 347 (1980).

[14] D. Pieroux and P. Mandel, Opt. Commun. **107**, 245 (1994).

[15] P.M. Alsing, V. Kovanis, A. Gavrielides, and T. Erneux, Phys. Rev. A **53**, 4429 (1996).

[16] K. Engelborghs, T. Luzyanina, K. in't Hout, and D. Roose, SIAM J. Sci. Comput. (to be published); K. Engelborghs, T. Luzyanina, and D. Roose, J. Comp. Appl. Math. **6** (2000); K. Engelborghs, ''DDE-BIFTOOL: a Matlab Package for Bifurcation Analysis of Delay Differential Equations,'' http://www.cs.kuleuven.ac.be/~koen/delay/ddebiftool.shtml

[17] P. Mandel, *Theoretical Problems in Cavity Nonlinear Optics* (Cambridge University Press, Cambridge 1997).

[18] C.L. Tang, H. Statz, and G. deMars, J. Appl. Phys. **34**, 2289 (1963).

[19] G.P. Agrawal, IEEE J. Quantum Electron. **QE-23**, 860 (1987).

[20] C.B. Su, J. Schlafer, and R.B. Lauer, Appl. Phys. Lett. **57**, 849 (1990).

[21] E.A. Viktorov and P. Mandel, Phys. Rev. Lett. **85**, 3157 (2000).

[22] E.A. Viktorov and P. Mandel, Opt. Lett. **25**, 1576 (2000).
[23] T. Erneux, G.H.M. van Tartwijk, D. Lenstra, and A.M. Levine, Proc. SPIE **2399**, 170 (1995).
[24] A.M. Levine, G.H.M. van Tartwijk, D. Lenstra, and T. Erneux, Phys. Rev. A **52**, R3436 (1995).
[25] A.G. Vladimirov, E.A. Viktorov, and P. Mandel, Phys. Rev. E **60**, 1616 (1999).
[26] J.Y. Wang and P. Mandel, Phys. Rev. A **52**, 1474 (1995).
[27] J.Y. Wang, P. Mandel, and T. Erneux, Quantum Semiclassic. Opt. **7**, 169 (1995).
[28] *Handbook of Mathematical Functions*, edited by M. Abromovitz and I.A. Stegun (Dover, New York, 1972).
[29] E. Hairer, S.P. Norsett, and G. Wanner, *Solving Ordinary Differential Equations*, 2nd ed. (Springer-Verlag, Berlin, 1992), Vol. 1.
[30] D. Pieroux, T. Erneux, A. Gavrielides, and V. Kovanis, SIAM J. Appl. Math. (to be published); D. Pieroux, T. Erneux, T. Luzyanina, and K. Engelborghs (unpublished).